J. Am. Ceram. Soc., 90 [12] (2007) 3915–3922
DOI: 10.1111/j.1551-2916.2007.01996.x

SEM/EDX characterization of the hydration products of belite cements from class C coal fly ash

Sara Goñi* and Ana Guerrero

Instituto de Ciencias de la Construcción "Eduardo Torroja"(CSIC)
Serrano Galvache, 4, 28033 Madrid, España.

Tel: +34 91 3020440 (ext. 284)
FAX: +34 91 3020700

E-mail: sgoni@ietcc.csic.es aguerrero@ietcc.csic.es

Abstract

This paper presents the microscopic characterization of two types of fly ash belite cements and their hydration products by means of scanning electron microscopy (SEM), energy-dispersive X-ray (EDX) microanalysis and X-ray diffraction analysis. The cements were obtained from ASTM class C coal fly ash by the hydrothermal-calcination route in water (FABC-2-W) and NaOH 1M solution (FABC-2-N). The hydration was studied during a period of 180 days at 21ºC and >95% rh. The results showed important incorporation of Al in the C-S-H gel and other minor elements, with presumable composition close to that of aluminium-tobermorite. The C-S-H composition of the FABC-2-W is more stable over the hydration time than that of the FABC-2-N cement. Portlandite is scantly formed during hydration.

Keywords: Hydration products, Belite cement, class C-coal-fly ash, SEM, EDX, XRD.

Acknowledgement: Funding for the present research was provided by the Minister of Science and Technology under Project nº MAT 2002-04023-CO3. The authors wish to thank the Thermal Station of Cercs (Catalonia) for the fly ash supplied.

I. Introduction

There are numerous studies on the reaction products of Portland cement with water. Among them, calcium silicate hydrate gel (C-S-H) garners the most attention due to its structural characteristics. C-S-H gel possesses a high specific surface and therefore a high binding capacity, which is the responsible for the cohesive properties of Portland-based cements.

However, there is less information available about the characteristics of the hydrated products of belite cements, in particular the type of C-S-H gel formed in the case of fly ash belite cement (FABC). The interest in this type of cements is due to its technological properties, as well as to its environmental advantages.

Fly ash belite cements, obtained from coal fly ash as secondary raw materials, contribute to the sustainable development of the construction industry. The high CaO content in the case of ASTM class C coal fly ash implies an extra-reduction in CO_2 emissions in comparison with the emissions of a traditional Portland cement clinker. Also, the energy consumption during the manufacturing process is strongly reduced (800ºC vs 1450ºC). The energy consumption in the case of grinding is eliminated. The natural raw materials are preserved and residues and their landfill are eliminated[1-5].

The main properties of these cements are the following: (i) slow hydration rate, for which the heat that is liberated is more gradual and retraction problems are avoided (ii) low portlandite ($Ca(OH)_2$) yield, which assures good durability in the aggressive

atmospheres in which expansive reactions with $Ca(OH)_2$ could take place, and (iii) low pH of its pore solution. Based on these properties, these cements can be used, among others, for the construction of large dams and industrial and radioactive waste treatment facilities[6-12].

For all the above mentioned applications, we are investigating fly ash belite cements, in which ASTM class F and C coal fly ash from different Spanish power stations is being used as secondary raw material. The main aim of the present paper is the microscopic characterization of two types of fly ash belite cements and their hydration products by means of scanning electron microscopy (SEM), energy-dispersive X-ray (EDX) microanalysis and X-ray diffraction analysis.

II. Experimental Procedure

Spanish coal fly ash with high Ca content (ASTM Class C), called FA-2, was used as raw material. The FA-2 came from the Spanish Thermal Station of Cercs (Catalonia). The coal used was a mixture of soft-coal (hulla in Spain) and lignite (58% imported, 38% from Pedraforca (Catalonia) and 4% from Mequinenza (Teruel), The chemical composition of the FA-2 determined according to the Spanish standard UNE-EN 196-2, is given in Table 1. The FA-2 is in accordance with the requirements of ASTM Class C and the EN-UNE 450 specifications (SiO_2+Al_2O_3+Fe_2O_3 contents lower than 70%, high CaO content and a CaO/SiO_2 molar ratio of 1). The mineralogical composition of the FA-2 is given in Fig. 1 (a). The crystalline compounds are free lime (CaO), anhydrite ($CaSO_4$), quartz (SiO_2), hematite (Fe_2O_3), magnetite (Fe_3O_4), and mullite (A_3S_2) ($Al_6Si_2O_{13}$). An amorphous halo appeared between the 15 and 35 2θ angular zone, which corresponds to the glassy component of fly ash.

The fabrication process of the fly ash belite cement, called FABC-2, has two steps. A mixture of FA-2 and commercial CaO having a Ca/Si molar ratio of 2 was first hydrothermally treated in a demineralised water and 1M NaOH solution at a solution-to-solid ratio of 3:1, for 4 h at 200ºC and 1.24 MPa pressure with continuous stirring. In the case of the hydrothermal treatment in NaOH, the solid obtained after filtration was washed 3 times with demineralised water to eliminate excess NaOH.

In a further step, the dried solid (heated at 80ºC overnight) was heated at a rate of 10ºC/min up to 600ºC and at 5ºC/min from 600ºC to 800ºC. After heating at 800ºC, the cements were rapidly cooled in air down to the ambient temperature. The chemical compositions of the two cements, called FABC-2-W and FABC-2-N for demineralised water and NaOH, respectively, are given in Table I.

A commercial water reducer additive (Rheobuild-1000) in a proportion of 2% (by weight of cement) was used to prepare pastes having a demineralised water-to-cement ratio of 0.68 and 0.82 for FABC-2-W and FABC-2-N, respectively. These cements demand a great amount of water due, among others factors, to their great fineness (6.4 m^2/g and 5.5 m^2/g for FABC-2-W and FABC-2-N, respectively). The introduction of the additive decreased the water demand by 15%.

After mixing, prisms were molded into 1x1x6 cm specimens and compacted by vibration. The samples were demolded after 1 day at > 95% rh and cured at 21ºC under > 95% rh in sealed containers for a period ranging from 1 to 180 days after mixing. Prior to characterization study, part of samples was cut in monolithic pieces of about 10 mm

and dried at room temperature in desiccators with silica gel, up to a constant weight, to eliminate free water (evaporable water) and prevent decomposition of the C-S-H gel.

The hydrothermal treatment was carried out with a Parr model 4522 1000 mL pump with split-ring closure and a PID model 4842 temperature controller. XRD patterns were recorded on a Philips PW 1730 diffractometer with a graphite monochromator and using Cu $K\alpha_1$ radiation. SEM analysis was performed with a Jeol 5400 instrument equipped with an Oxford ISIS model energy dispersive X-ray spectroscopy module (EDX). The samples were covered with carbon by sputtering. SEM/EDX semiquantitative analyses were made with an accelerating voltage of 20 kV and a reference current of 300 μA on powder samples for determining the alkaline, alkaline-earth, iron oxides, alumina, silica and sulphur content. The EDX microanalysis has been carried out in spot mode over each different crystalline phase from areas of approximately 300 nm, given the detection limit of 0.2%. Thermal analyses were recorded with a Netzsch STA 409 simultaneous analysis system using 50 mg samples and a dynamic nitrogen stream (flow rate= 100 cm^3/min) with a heating rate of 10ºC/min.

III. Results and Discussion

(1) X-Ray Diffraction

(1.1) Hydrothermal treatment of fly ashes: synthesis of cement precursors

When FA-2 is hydrothermally treated in water at 200ºC (Fig. 1 (b)), all the reflections of the initial FA-2 disappeared (katoite ($Ca_3Al_2(SiO_4)(OH)_8$) and α-C_2SH ($Ca_2SiO_4.H_2O$) being the hydrated crystalline precursors formed). In the case of hydrothermal treatment in 1M NaOH solution (Fig.1 (c)), portlandite ($Ca(OH_2)$) and calcite ($CaCO_3$) from lime were formed together with katoite ($Ca_3Al_2(SiO_4)(OH)_8$).

The α-C_2SH precursor has a crystalline structure similar to that reported by Heller[13], who hydrothermally synthesized it by heating β-C_2SH at 150°C for 40 days. Ishida et al.[14] hydrothermally prepared α-C_2SH in 2 h at 200°C from a mixture of lime and silicic acid. The α-C_2SH dissociates at 390-490ºC through a two-step process, to form an intermediate phase plus some γ-C_2S. This compound appears to be a new dicalcium silicate different from known dicalcium silicate (α, α_L' , α_H' β and γ phases). At 920-960ºC, all the phases are transformed to the α_L' phase. The intermediate phase has high crystallinity and is stable at room temperature[14].

Another hydrated precursor of the β-C_2S polymorph is hillebrandite ($Ca_2(SiO_3)(OH)_2$), which was synthesized by Ishida et al.[15] from a mixture of quartz or silicic acid and lime; the mixture was hydrothermally treated at 200ºC for 10h or at 250ºC for 5 h. On heating, hillebrandite starts to decompose at about 500°C and produces low-crystalline β-C_2S, which is stable at room temperature and has a remarkably large specific surface area of about 7 m^2 /g. The decomposition reaction rate in a single crystal is rapid, and the reaction is considered to proceed topotactically.

In our case, heating the hydrated precursors (HT-2-W) obtained after hydrothermal treatment of FA-2 in water (Fig. 2) produced a first weight loss, with a maximum at 160ºC in the DTG curve, which could be attributed to the C-S-H decomposition. A second weight loss between 300ºC and 580ºC, which gives a DTG peak centred at 460ºC and a shoulder centred at 380ºC, could be attributed to decomposition of both α-C_2SH and portlandite ($Ca(OH)_2$). Assuming that no portlandite is present in the sample (as the corresponding XRD pattern showed (Fig. 1 (b)) and that the weight loss in the two steps between 300ºC and 580ºC is due to α-C_2SH

dehydration as Ishida et al. pointed out[14], the α-C_2SH content would be 90%. The calcite content is 4.5%. This content was determined from the weight loss in the TG curve between 680ºC and 780ºC and its percentage is 4.5%.

In the case of the precursors obtained from the HT-2-N, in which no α-C_2SH appeared, the content of portlandite is 43% and the content of calcite is 19%. The portlandite percentage was determined from the weight loss in the TG curve between 300ºC and 500ºC (Fig. 2), and that of calcite from the weight loss in the TG curve between 600ºC and 780ºC.

(1.2) Anhydrous Fly ash Belite cements

The FABCs were obtained after heating the precursors at 800ºC. This temperature was considered optimal, according to previous work[1].

In the case of anhydrous FABC-2-W (Fig. 1 (d)), broad reflections appeared in the 32-33 2θ angular zone, which corresponds to the $\alpha`_L$-C_2S (Ca_2SiO4) belite variety with poor crystallinity; gehlenite (C_2AS) ($Ca_2Al_2SiO_7$), traces of mayenite ($C_{12}A_7$) ($Ca_{12}Al_{14}O_{33}$) and calcite (Cc) ($CaCO_3$) were also detected. The main differences observed in the case of anhydrous FABC-2-N cement (Fig. 1 (e)) are the following: (i) higher intensity and better definition of the $\alpha`_L$-C_2S (Ca_2SiO_4) peaks and (ii) lower calcite and higher mayenite contents. The absence of free lime in the two cements suggested a 100% reaction. Calcite content (determined from thermogravimetric analysis) was 1.1% and 2.3% for the FABC-2-W and FABC-2-N respectively.

It is interesting to note the high fineness of both cements (6.4 m^2/g and 5.5 m^2/g for FABC-2-W and FABC-2-N, respectively) which are obtained without grinding.

The $\alpha`_L$-$C_2S$ obtained at 800ºC comes from the $\alpha$-$C_2SH$ precursor in the case of the HT-2-W. According to Ishida et al.[14], the intermediate and unidentified $C_2S$ crystalline phase, formed after dehydration of $\alpha$-$C_2SH$ at 493ºC, transformed to the $\alpha`_L$-C_2S phase at 920ºC-960ºC. In our case, no intermediate crystalline phase was formed from precursor dehydration.

(1.3) Hydrated products after 180 days of hydration at 20ºC

The hydrated compounds having poor crystallinitity were (Fig. 1 (f)) the following: hydrated calcium-monosulpho-aluminate (C_4AsH_{10}) ($[Ca_2Al(OH)_6H_2O]_2SO_4 \cdot 5H_2O$) of the lamellar AFm structural type[16] and $C_2SH_{0.35}$ ($Ca_2SiO_4 \cdot 0.35H_2O$). Some of the peaks from the C-S-H gel at 3.04 Å, 2.79 Å, and 1.82 Å[16, 17] could also be present, together with traces of portlandite (CH) ($Ca(OH)_2$).

The main differences observed in the case of the hydrated products of the anhydrous FABC-2-N cement (Fig. 1 (g)) are as follows: (i) the intensity of $\alpha`_L$-C_2S (Ca_2SiO_4) almost disappears, suggesting a higher hydraulic reactivity for this cement; (ii) no portlandite appeared, and (iii) a double peak is detected in the interlayer space of the lamellar hydrated calcium-monosulpho-aluminate (C_4AsH_{10}) centred at 10.86 and 11.73, respectively, of the 2θ angular zone. This fact seem to indicate SO_4^{2-}/CO_3^{2-} substitution due to a partial carbonation of the (C_4AsH_{10}) and formation of the hydrated calcium-monocarbo-aluminate (C_4AcH_{11}) ($[Ca_2Al(OH)_6H_2O]_2CO_3 \cdot 6H_2O$).

(2) Scanning electron Microscopy and X-ray microanalysis

Wide microscopic and X- ray microanalyses of the main representative crystals were made on the initial FA-2, anhydrous FABC-2-W, and FABC-2-N cements; hydrated products formed after 28, 90, and 180 days of hydration at 21ºC, respectively.

(2.1) Starting fly ash (FA-2) and anhydrous FABC-2 cements

The different sized spherical particles (cenospheres) of initial FA-2 can be seen in Fig. 3 (a, b). Different sized plates, and small rounded particles are detected in the case of anhydrous FABC-2-W (Fig. 4 (a-c)) and FABC-2-N cements (Fig. 4 (d-f)).

The principal results for individual microanalysis from varying parts of the samples are presented as a plot of the atom ratios of Si/Ca vs Al/Ca in Fig. 5. In this figure, the ideal atom ratios for the crystalline compounds detected from XRD are included. In the case of the initial FA-2, the Al/Ca and Si/Ca atom ratio values arranged in a diagonal line, which indicated similar Si/Ca and Al/Ca atom ratio values. The corresponding Si/Ca values for both FABC-2-W and FABC-2-N anhydrous cements arranged around 0.5, the theoretical Si/Ca atom ratio of ideal belite and gehlenite. The Al/Ca values ranged from 0.05 to 1. The higher Al/Ca values corresponded to the small rounded particles in both cements attributable to gehlenite. The mean compositions of the more representative crystals are given in Table II. From these results, the mean unit formula compositions calculated as Ca_2SiO_4 in the case of plates were:

FABC-2-W: $Ca_{1.586}\,Mg_{0.016}\,Na_{0.011}\,K_{0.089}\,Si_{0.978}\,Al_{0.183}\,Fe_{0.024}\,S_{0.027}\,O_4$ and

FABC-2-N: $Ca_{1.528}\,Mg_{0.012}\,Na_{0.285}\,K_{0.048}\,Si_{0.816}\,Al_{0.357}\,Fe_{0.027}\,S_{0.028}O_4$

As can be seen, the belite phase is impure and contains considerable amounts of other elements which come from the starting fly ash, such as Al, Fe, S, Mg, Na and K.

In the case of FABC-2-N cement, the content of Al is higher than that of FABC-2-W while the content of Si is lower. The difference indicates an almost 1:1 molar substitution of Si^{4+} by Al^{3+}; the charge difference seems to be balanced by Na^{+}, whose content is 26 times higher than that in FABC-2-W. The mean unit formula compositions of the smaller rounded particles, calculated as $Ca_2 Al_2 SiO_7$ were:

FABC-2-W: $Ca_{2.332} Mg_{0.012} Na_{0.039} K_{0.130} Si_{1.300} Al_{1.083} Fe_{0.047} S_{0.092} O_7$ and

FABC-2-N: $Ca_{1.963} Na_{0.574} K_{0.062} Si_{1.243} Al_{1.373} Fe_{0.040} S_{0.038} O_7$

Similarly as in the case of belite, Si, Fe, and S content decreased as Al increased, for the gehlenite-like phase of FABC-2-N cement, the charge difference being balanced by Na^{+}, whose content is 15 times higher than that in FABC-2-W.

It is difficult to compare these results with the bibliography data due to the different routes used for synthesizing belite. For example, in our case, the temperature for the synthesis of belite cements was 800ºC, at which the fusion of phases is not reached (which is important to be considered from the point of view of diffusion and ionic substitutions). Thus, the inclusion of elements other than Si and Ca in the belite occurs during the hydrothermal treatment where the precursors were formed. Herfort et al.[8], reported the following unit formula compositions for two low-energy cements based on rich belite clinker obtained at 1300ºC with a partial fusion of raw materials:

$Ca_{1.965} Mg_{0.015} Na_{0.010} K_{0.005} Ti_{0.005} Si_{0.830} Al_{0.080} Fe_{0.030} S_{0.050} P_{0.010} O_4$ and

$Ca_{1.950} Mg_{0.015} Na_{0.010} K_{0.005} Ti_{0.005} \square_{0.015} Si_{0.805} Al_{0.085} Fe_{0.030} S_{0.070} P_{0.010} O_4$

Where $\square$ denotes a vacant on the Ca octahedral site. The apparent 1:1 molar substitution of Si by S in the tetrahedral sites was related to an increase in sulphate activity (SO_3/alkali ratio) and mechanical strength development. The charge was balanced through the development of vacancies on the Ca sites.

(2.2). Hydration products in FABC-2 pastes

The morphologies of the main hydrated products of FABC-2-W and FABC-2-N cement pastes cured for 180 days are given in Fig. 6.

The particles consistent with C-S-H composition appear fibrous in FABC-2-W hydrated for 90 days (Fig. 6 (a)) and they later transform into dense aggregates of globular morphology (Fig. 6 (b)). This morphological transformation is not produced in the case of FABC-2-N, where the C-S-H gel already appears like dense aggregates of globular morphology starting after 28 days of hydration (Fig. 6 (c)).

The fine plates of high Ca content detected in the case of FABC-2-W after 28 days of hydration (Fig. 6 (d)), could represent mixtures of C-S-H with portlandite. This mixture can not be resolved by conventional scanning or transmission electron microscopy methods[18-20]. In the case of FABC-2-N, no portlandite plates are detected after 28 days or at a later date after further hydration. The lack of portlandite agrees with the XRD result of Fig. 1. Most likely Ca precipitated into a Ca-rich phase of the AFm (C_4As,cH_x) type instead of portlandite.

The hexagonal plates, which grow mainly in pores of the FABC-2-N paste (Fig. 6 (e)), have an Al/Ca atom ratio value of 0.5 and Si/Ca atom ratio value of 0 (attributed to the theoretical composition of the AFm-like phases). The corresponding S/Ca contents are below 0.25, which suggests hydrated calcium-monocarbo-aluminate composition ($[Ca_2Al(OH)_6H_2O]_2CO_3.9H_2O$).

Besides Ca and Si, the C-S-H gel contains considerable amounts of Al, Fe and other elements. The composition (mean atoms relative to Ca) of the C-S-H gel as a function of the hydration time and type of cement is given in Table III.

With respect to the hydration time, the variations of the relative elemental composition of the C-S-H gel of FABC-2-W are less evident than those of the FABC-2-N. In the later cement, a remarkable decrease of the Na/Ca ratio (from 0.11 to 0.022) is observable from 28 days to 180 days of hydration; the Si/Ca atom ratio increases from 0.63 to 0.75, while the dispersion of Mg/Ca values make it impossible to establish any valid conclusions.

For a fixed hydration time, the C-S-H gel of the FABC-2-N cement has the following characteristics in comparison with those of FABC-2-W: the Na/Ca and Si/Ca ratios are higher whereas the S/Ca, Al/Ca, and Fe/Ca ratios are lower, and the mean Al/Ca ratio is near 0.2 for C-S-H gel of FABC-2-W, while that of FABC-2-N is near 0.13. The low Al/Ca content of C-S-H gel in FABC-2-N could be attributed to its liberation and incorporation in the AFm-like crystals of Fig. 6e. An increase in AFm was also observed by Love et al.[21] in alkali activated pastes of white Portland cement blended with 20% of metakaolin (MK). In any case, our Al/Ca atom ratios values are considerably higher than those reported based on SEM/EDX results for the C-S-H gel of Portland cement (Al/Ca = 0.07)[18-20, 22], and are close to those of C-S-H formed from hydration of Portland cement blended with slags (0.2)[23-25].

It is accepted that Al substitutes Si in the chains of C-S-H, nevertheless, in our case, Al and Fe also substitute Si as can be deduced from Fig. 7. An inverse linear correlation is obtained when Al+Fe is plotted vs Si. This correlation is general and

extensive to all the C-S-H microanalyses, irrespective of the hydration time and type of FABC cement. The regression coefficient (R^2 = 0.90) was the higher compared with that reached when Al (R^2 = 0.87) or Al+Fe+S (R^2 = 0.83) was plotted vs Si.

As can be seen in Table III, the maximum substitution of Si by Al+Fe is 33% and 21% for FABC-2-W and FABC-2-N, respectively. These results are consistent with those reported in the literature [21, 23, 26, 27] taking into account that in our case Fe was incorporated into the atom ratio.

Love et al. [21] studied the microstructure and composition of water- and alkali-activated hardened pastes of white Portland cement–20% metakaolin blends using solid-state NMR spectroscopy and analytical TEM. The results showed that when the high degree of reaction of the MK at 28 days in both pastes resulted in long-chain highly aluminous C–S–H, with most of the bridging sites occupied by Al^{3+} rather than Si^{4+}. The data for the C–S–H in the water-activated paste are consistent with both the tobermorite/jennite (T/J) and tobermorite/calcium hydroxide (T/CH) models for the nanostructure of C–S–H. Although very little J- or CH-like structure is needed to account for the observed compositions, whilst those for the alkali-activated paste can only be accounted from the T/CH viewpoint. The high substitution of Si by Al (34%) was reached in the case of alkali activated pastes vs only 24% for water activated pastes. They found a direct linear correlation between the degree of polymerization of the chains and the Al substituted. So, the mean chain length (MCL) was 15.7 and 11.0 for 34% and 24% Al/Si substitution, respectively.

In our case, an attempt was made for estimating the variations of the mean chain length (MCL) of C-S-H on the basis of results reported in Table 2 of Love et al.[21]. If the

MCL values are plotted vs the Al/Si values, the following direct linear regression is obtained:

$$MCL = 40.3(Al/Si) - 0.12 \quad (R = 0.87) \qquad [1]$$

According to this equation and our (Al+Fe)/(Si+Al+Fe) values, we estimated the MCL values, which, together with the corresponding compressive strength values, were included in Table III. As can be seen, in general, the MCL values are lower for the FABC-2-N cement. There is no clear correlation between the MCL values of C-S-H gel and compressive strength. We believe that other microstructural, packing or density factors could be better related to mechanical strength than MCL, as was reported by us in an unpublished work[28].

Faucon et al.[26] based on the C-S-H structure like that of tetrahedral-octahedral-tetrahedral (Te – Oc - Te) of smectite (where the Te sheets of SiO_2 linear chains are associated to a “pseudo-octahedral sheet of CaO as the tobermorite structure), pointed out that the Al incorporation in the chains depends on the Ca/Si ratio. Therefore, two structures called C-S-Ha and C-S-Hb are produced for low (0.66) and high (1.5) Ca/Si ratios, respectively. In the case of C-S-Ha, the tetrahedral sheet is formed by linear silicate chains, where Al^{3+} substitutes Si^{4+} in the nonbridging position of the chains for Al(IV)/[Si + A(IV)] lower than 0.22. For Al(IV)/[Si + A(IV)] higher than 0.22 in the C-S-Ha, a redistribution of the aluminium between the bridging and nonbridging positions might occur.

When the Ca/Si ratio is high, the Al position in the nonbridging tetrahedron is unstable, provoking the rupture of the chains and changing the structure of the C-S-H from C-S-Ha to C-S-Hb; the bridging positions become the preferential substitution site for aluminum. Progressive substitution of Ca^{2+} by Al^{3+} in the octahedral sheet is

observed. When the tetrahedral sheet is constituted of dimer structure like C-SHb, there is no Si^{4+} substitution, but instead, Ca^{2+} substitution in the interlayer space (5-fold coordinated) and in the octahedral sheet. Such a substitution remains, however, limited compared to Si^{4+} substitutions. The amount of aluminum incorporated in the C-S-H structure increases with the length of the chains.

In our case, it is not possible to distinguish the coordination degree of the Al. However, the substitution of Si by Al+Fe deduced from the results of Fig. 7 indicates a tetrahedral coordination. The substitution of Ca^{2+} by Al^{3+} in the octahedral sheet is discarded. This conclusion can be deduced from the results of Fig. 8, where a direct linear correlation is obtained when the (Al+Fe)/(Si+Al+Fe) atom ratio is plotted vs the Ca/Si atom ratio.

Sun et al.[27] studied by X-ray diffraction, compositional analysis, and ^{29}Si and ^{27}Al MAS NMR spectroscopy, the structural mechanisms of Al-substitution in Al-substituted tobermorite-type C–S–H made by precipitation from solution. The results lead to an overall model for incorporation of Al in tobermorite-type C–S–H that has several interesting features. (1) The structural core of the tobermorite-type layers, consisting of the central Ca–O sheet and the pairing tetrahedra, is essentially unmodified by Al incorporation (2) Al[4] occurs on the bridging tetrahedral of the drierkette chains with both Q2 and Q3 linkages, and is charge balanced by alkali cations, Al[5] and Al[6], and possibly Ca^{+2} and H^{+} (3) The Al[5] and Al[6] occur in hydrous aluminate, Ca-aluminate, or Na-aluminate environments associated with C–S–H in the interlayer galleries and/or on the particle surfaces. The polymerization of the alumino-silicate drierkette chains increases with increasing Al/(Si+Al) ratio as Al enters the bridging tetrahedral sites and

links portions of the aluminosilicate chains that are disconnected at lower Al-contents. The maximum total Al/(Si+Al) ratio in the C–S–H was about 23%.

In respect to the Na position, it is interesting to note that the samples prepared by Sun et al.[27] have significant levels of Na that cannot be removed by washing in water, indicating that Na plays an important charge balancing role. Na occurs on sites that allow it to become mobile when the sample is wet (probably surface sites) and also on sites that are rigidly held in the structure (probably interlayer sites). In our case, the decrease of Na with time (produced in the alkali activated FABC-2-N C-S-H gel) could be explained if mobile Na is located at the surface sites.

With respect to the position of Al and Fe in the silicate chains, it is not possible to conclude if Al and Fe substitutes Si in the central tetrahedra bridges of the dreierkette, the nonbridging sites, or both as Faucon et al. explained[26] . To dicover the substitution location, studies using ^{29}Si and ^{27}Al MAS NMR are needed, which we hope to conduct in the near future.

With respect to the S incorporation in the C-S-H gel, the same considerations as in the case of Portland cement could be made. According to Famy et al.[19] S is adsorbed as $SO_4^=$ and not chemically bounded, requiring Ca^{2+} to balance the negative charge; nevertheless, Taylor[18] and Richardson and Groves[20] considered that S coming from the AFm and AFt phases are intimately mixed together with $Ca(OH)_2$ and the tobermorite layers. In any case, if S is adsorbed as $SO_4^=$ its possible liberation to the pore-solution could play an important role from the delayed ettringite formation point of view.

IV. Conclusions

- Big plates consistent with the ideal belite composition are detected in the anhydrous FABC-2-W and FABC-2-N cements, Na, K, Mg, Al, Fe and S are incorporated into their compositions according to the following atom per unit formulas:

  FABC-2-W: $Ca_{1.586}\,Mg_{0.016}\,Na_{0.011}\,K_{0.089}\,Si_{0.978}\,Al_{0.183}\,Fe_{0.024}\,S_{0.027}\,O_4$ and

  FABC-2-N: $Ca_{1.528}\,Mg_{0.012}\,Na_{0.285}\,K_{0.048}\,Si_{0.816}\,Al_{0.357}\,Fe_{0.027}\,S_{0.028}O_4$.

- Unlike the C-S-H gel of hydrated Portland cement pastes, the C-S-H gel of these hydrated belite cements contained elements such as Fe, Na, K, S and Mg in higher amounts than Si and Ca. Substitutions of Si by Al and Fe take place.
- The high Al content favours a composition of the C-S-H gel closed to that of aluminium-tobermorite.
- Taking into account the (Al+Fe)/(Si+Al+Fe) atom ratio, the maximum substitution of Si by Al and Fe was 33% and 21% for FABC-2-W and FABC-2-N, respectively.
- According to these data and the linear regression equation from Table 2 of reference 21, the corresponding mean chain lengths (MCL) were 13 and 8 for FABC-2-W and FABC-2-N, respectively.
- There does not exist a clear correlation among the MCL values of C-S-H gel and the corresponding compressive strength values. We believe that other microstructural factors such as packing, density, and surface factors could be better related to mechanical strength than MCL.
- The low Al/Ca content of the C-S-H gel of FABC-2-N (0.13) in comparison with that of FABC-2-W (0.20) is attributed to its liberation and incorporation in the AFm-like crystals; the higher Si/Ca atom ratio values observed in the FABC-2-N could be attributed to the lower Si substitution by Al and Fe.

References

[1] A. Guerrero, S. Goñi, I. Campillo and A. Moragues, "Belite cement clinker from coal fly ash of high Ca content. Optimization of synthesis parameters". *Environ. Sci. and Technol.* **38 [11],** 3209-3213 (2004).

[2] S. Goñi Elizalde, A. Guerrero Bustos, A. Moragues Terradas, M.F. Tallafigo Vidal, I. Campillo Santos, J. Sánchez Dolado, and A. Porro Fernández, "New belite cement clinkers from fly ash of coal combustion of high Ca content". Spanish Patent ES2199059 (2005).

[3] S. Goñi, A. Guerrero and M.P. Lorenzo, "Microscopy study of belite phases obtained from coal fly ash class C: Influence of heating". In Proceedings of 10th Euroseminar on Microscopy Applied to Building Materials, Pasley, (ed. by J.J. Hughes, A.B. Leslie and J.A. Walsh), University of Pasley, Scotland (2005).

[4] A. Guerrero, S. Goñi, A. Moragues, and J.S. Dolado, J.S. "Microstructure and mechanical performance of belite cements from high calcium coal fly ash" *J. Am. Ceram. Soc.* **88 (7),** 1845-1853 (2005).

[5] S. Goñi and A. Guerrero, "Influence of coal fly ash class C alkaline hydrothermal activation on belite cement hydration. Surface area and pore-size distribution study" Proceedings of the 12th International Congress on the Chemistry of Cement (to be published).

[6] A.K. Chatterjee, "High belite cements-present status and future technological options: Part I". *Cem. Concr. Res*. **26 [8],** 1213-1225 (1996).

[7] A.K. Chatterjee, "Future technological options: Part II". *Cem. Concr. Res*. **26 [8],** 1227-1237 (1996).

[8] D. Herfort, A.S. Holmboe, U. Costa, E. Gotti, and S. Grundvig, "High strength, low energy cement based on belite rich clinker". In Proceedings of the 8th Euroseminar on Microscopy in Building Materials, Athens, September 4-7, pp 139-146 (2001).

[9] S-H. Guo, H-T Zhang, L. Zhen, W-S. Zhang, and Y-M Chen, "The formation and performance of high belite cement clinker with different interstitial phase content". In Proceedings of the 11th International Congress on the Chemistry of Cement (ICCC) "Cement´s Contribution to the Development in the 21st Century", (ed. by G. Grieve and G. Owens), pp. 1027-1034 (2003). Durban, South Africa.

[10] E. Gartner, “Industrially interesting approaches to “low-CO_2” cements”. *Cem. Concr. Res*. **34,** 1489-1498 (2004).

[11] A. Guerrero and S. Goñi, “Long term durability of High Coal Fly Ash Belite Cement-Mortar exposed to sulphate attack at 40ºC”, Proceedings of the 12th International Congress on the Chemistry of Cement (to be published).

[12] S. Goñi and A. Guerrero, “Efficiency of fly ash belite cement and zeolite matrices for immobilizing cesium”. *J. Hazard. Mater* ***137*** **[3]**, 1608-1617 (2006).

[13] L. Heller, “The structure of dicalcium silicate α-hydrate”, *Acta Crystallogr*. **5** 724–728 (1952).

[14] H. Ishida, S. Yamazaki, K. Sasaki, Y. Okada, T. Mitsuda, “α-Dicalcium silicate hydrate: Preparation, decomposed phase, and its hydration”, *J Am Ceram Soc* **76 (7)** 1707–1712 (1993).

[15] H. Ishida, K. Mabuchi, K. Sasaki and T. Mitsuda, “ Low-Temperature synthesis of β-Ca_2SiO_4 from hillebrandite” *J Am Ceram Soc* **75 (9)** 2427-2432 (1992).

[16] H.F.W. Taylor, “Hydrated aluminate, ferrite and sulphate phases in cement chemistry (ed. by H.F.W. Taylor), pp 167-198 (1992). Academic Press, London.

[17] C. Röβler and J. Stark, “Limited-dose Electron Microscopy reveals the crystallinity of fibrous C-S-H phases”, *J. Am. Ceram. Soc*. **89 (2**), 627-632 (2006).

[18] Harry F. W. Taylor, “Proposed structure for calcium silicate hydrate gel”. *J. Am. Ceram. Soc*. **69 [6]** 464-67 (1986).

[19] C. Famy, A.R. Brough and H.F.W. Taylor, “The C-S-H Gel of Portland cement mortars: Part I. The interpretation of Energy-Dispersive X-Ray Microanalyses from Scanning Electron Microscopy, with some observations on C-S-H, AFm and AFt phase compositions”. *Cem. Concr. Res*. **33**, 1389-1398 (2003).

[20] I.G. Richardson and G.W. Groves, “Microstructure and microanalysis of hardened ordinary Portland cement pastes”. *J. Mater. Sci.* **28**, 265-277(1993).

[21] C.A. Love, I.G. Richardson, A.R. Brough, “Composition and Structure of C-S-H in White Portland Cement – 20% Metakaolin Pastes Hydrated at 25°C”*, Cem. Concr. Res.* **37** 109-117 (2007).

[22] I.G. Richardson and G.W. Groves, "The incorporation of minor and trace elements into calcium silicate hydrate (C-S-H) gel in hardened cement pastes". *Cem. Concr. Res*. **23,** 131-138 (1993).

[23] I.G. Richardson, "Tobermorite/Jennite-and Tobermorite/Calcium Hydroxide-based models for the structure of C-S-H: Applicability to hardened pastes of tricalcium silicate, β-dicalcium silicate, Portland cement, and blends of Portland cement with blast-furnace slag, metakaolin, or silica fume". *Cem. Concr. Res.* **34,** 1733-1777 (2004).

[24] I.G. Richardson, A.R. Brough, R. Brydson, G.W. Groves and C.M. Dobson, "Location of aluminum in substituted calcium silicate hydrate (C-S-H) gel as determined by ^{29}Si and ^{27}Al NMR and EELS". J*. Am. Ceram. Soc*. **76 (9),** 2285-88 (1993).

[25] S.D. Wang and K.L. Scrivener, "^{29}Si and ^{27}Al NMR study of alkali-activated slag", *Cem. Concr. Res.* **33,** 769-774 (2003).

[26] P. Faucon, A. Delagrave, J.C. Petit, C. Richet, J.M. Marchand, H. Zanni, "Aluminum Incorporation in Calcium Silicate Hydrates (C-S-H) Depending on their Ca/Si Ratio", *J. Phys. Chem.* **B 103** 7796-7802 (1999).

[27] G.K. Sun, J.F. Young, R.J. Kirkpatrick, "The Role of Al in C-S-H: NMR, XRD, and Compositional Results for Precipitated Samples", *Cem. Concr. Res.* **36** 18-29 (2006).

[28] S. Goñi and A. Guerrero, "Influence of two types of C-S-H gel on the mechanical strength of belite cements from coal fly ash Class C" (in preparation).

LIST OF CAPTIONS

Figure 1. X-ray diffraction patterns of the starting fly ash (FA-2), cement precursors (HT-2-W and HT-2-N, anhydrous cements (FABC-2-W and FABC-2-N) and hydrated for 180 days.

Figure 2. TG and DTG curves of hydrated precursors HT-2-W and HT-2-N

Figure 3. SEM images of starting fly ash (FA-2).

Figure 4. SEM images of anhydrous FABC-2-W (a-c) and FABC-2-N (d-f) cements.

Figure 5. Al/Ca vs Si/Ca atom ratio for the starting FA-2; anhydrous FABC-2-W and FABC-2-N cements.

Figure 6. SEM images of hydrated FABC-2-W and FABC-2-N pastes.

Figure 7. Al+Fe vs Si atom ratio from spot X-ray microanalyses of C-S-H gel of hydrated FABC-2-W and FABC-2-N pastes (Table III).

Figure 8. (Al+Fe)/Si vs Ca/Si atom ratio from spot X-ray microanalyses of C-S-H gel of hydrated FABC-2-W and FABC-2-N pastes (Table III).

Table I. Chemical Composition of the Starting Fly Ash (FA-2) and Anhydrous FABC-2-W and FABC-2-N Cements (% By Weight)

	LOI	CaO	SiO2 (total)	Fe2O3 (total)	Al2O3	MgO	SO3	Na2O	K2O	SiO2 (reactive)	BET (m2/g)
FA-2	4.0	32.0	32.8	4.2	19.3	2.2	2.8	0.44	1.6	25.2	3
FABC-2 W	1.4	48.3	28.7	2.3	15.2	1.4	1.7	0.25	0.5	28.6	6.4
FABC-2-N	2.7	48.3	23.6	3.0	14.4	1.2	1.2	4.5	0.38	23.5	5.5

Silica reactive according to Spanish standard UNE-80-224. LOI, loss on ignition; BET, Brunauer–Emmett–Teller.

Table II. Mean Compositions of the Main Regions of FABC Cements

Oxides (%)	SiO_2	Al_2O_3	Fe_2O_3 total	SO_3	CaO	Na_2O	K_2O	MgO	Total
FABC-2-W (20 total EDX analysis)									
Plates	35.36	5.64	1.16	1.29	53.43	0.22	2.52	0.39	100.00
Rounded	27.68	19.59	1.34	2.63	46.11	0.43	2.17	0.18	100.11
FABC-2-N (20 total EDX analysis)									
Plates	28.90	10.75	1.26	1.34	50.47	5.21	1.32	0.29	99.54
Rounded	26.41	24.81	1.14	1.07	38.94	6.30	1.03	0.00	99.72
	Si	Al	Fe	S	Ca	Na	K		Mg
Mean molar ratios relative to Ca									
FABC-2-W									
Plates	0.62 (7)	0.12 (6)	0.016 (15)	0.017 (4)	1.00	0.006 (5)	0.057 (9)		0.010 (5)
Rounded	0.57 (14)	0.48 (13)	0.022 (15)	0.041 (10)	1.00	0.018 (17)	0.057 (7)		0.005 (1)
FABC-2-N									
Plates	0.54(13)	0.24 (9)	0.021 (16)	0.018 (12)	1.00	0.20 (14)	0.032 (24)		0.00 (0)
Rounded	0.64 (6)	0.71 (12)	0.022 (16)	0.020 (8)	1.00	0.31 (22)	0.033 (26)		0.00 (0)

Standard deviation on final digits are in parentheses.
EDX, energy-dispersive X-ray.

Table III. Mean Atom Ratios Relative to Ca, (Al+Fe)/(Si+Al+Fe) Atom Ratios, MCL of C–S–H Gel and Compressive Strength

	Si	Al	Fe	S	Na	K	Mg	(Al+Fe)/ (Si+Al+Fe)	MCL	Rc (MPa)
FABC-2-W (30 total EDX analysis)										
28 days	0.52 (1)	0.22(6)	0.044 30)	0.053 (14)	0.014 (10)	0.020 (13)	0.092 (91)	0.33	13	17
90 days	0.63 (8)	0.17 (7)	0.027 (12)	0.060 (18)	0.017 (11)	0.010 (2)	0.033 (22)	0.23	9	23
180 days	0.57 (10)	0.22 (6)	0.021 (12)	0.050 (22)	0.015 (12)	0.011 (3)	0.024 (14)	0.29	12	26
FABC-2-N (30 total EDX analysis)										
28 days	0.63 (10)	0.13 (6)	0.019 (5)	0.009 (4)	0.11 (6)	0.016 (2)	0.027 (26)	0.19	8	19
90 days	0.62 (5)	0.15 (6)	0.017 (9)	0.015 (10)	0.058 (28)	0.012 (4)	0.014 (1)	0.21	8	19
180 days	0.75 (2)	0.11 (3)	0.016 (8)	0.017 (2)	0.022 (5)	0.009 (3)	0.026 (3)	0.14	6	19

Standard deviation on final digits are in parentheses.
MCL, mean chain length, calculated according to data of Love et al. 21
EDX, energy-dispersive X-ray.

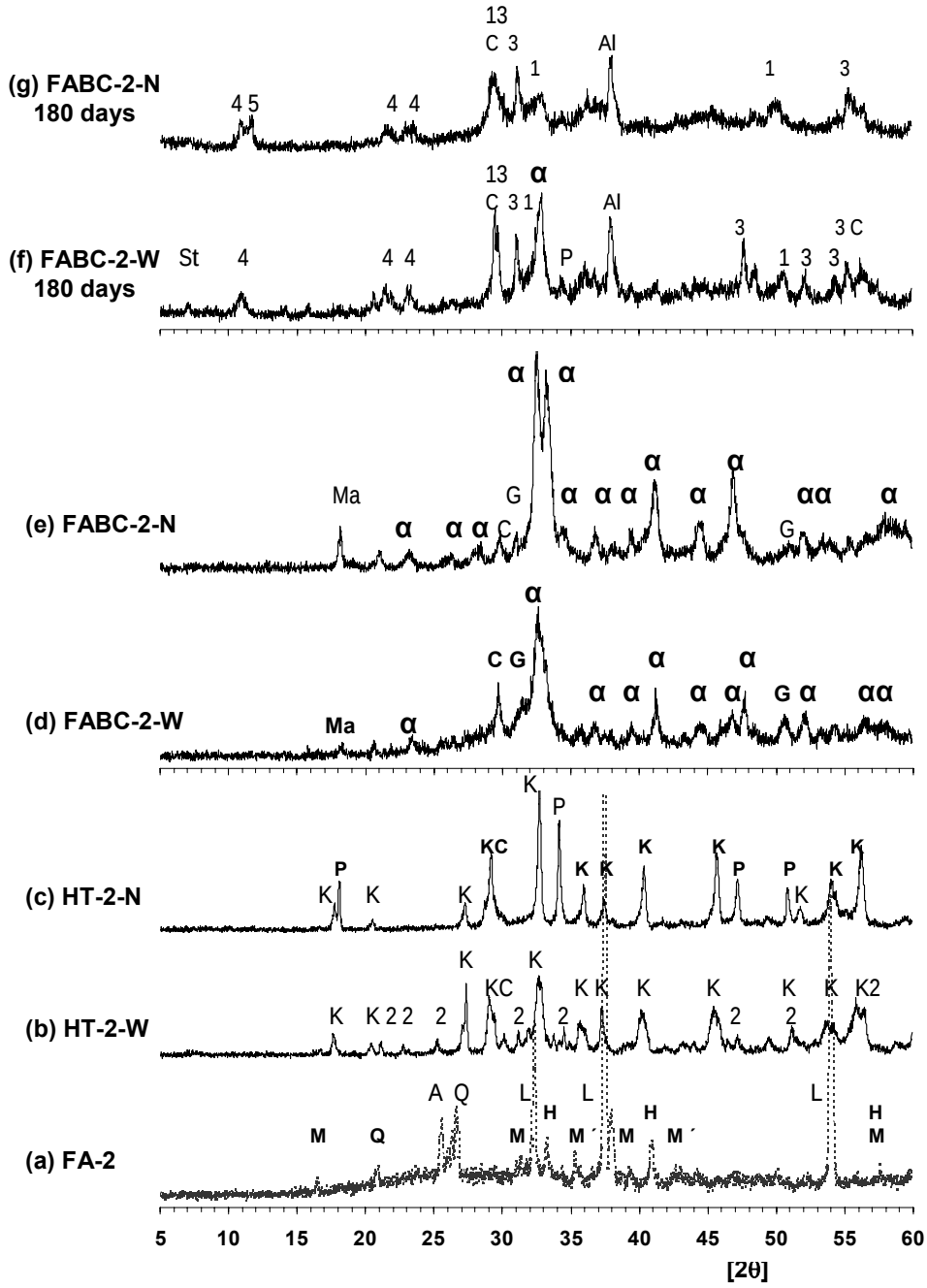

A anhydrite; Q quartz; M mullite; L lime ; H hematite C calcite; Ma mayenite; M´magnetite; α α´$_L$-C_2S; G gehlenite; 1 $C_{1.5}SH_x$; 2 α-C_2SH; 3 $C_2SH_{0.35}$; 4 C_4AsH_{10} (monosulfo); 5 C_4AcH_{11}; Al aluminum from sample holder; K katoite; P portlandite.

Figure 1. X-ray diffraction patterns of the starting fly ash (FA-2), cement precursors (HT-2-W and HT-2-N), anhydrous cements (FABC-2-W and FABC-2-N) and hydrated cements for 180 days.

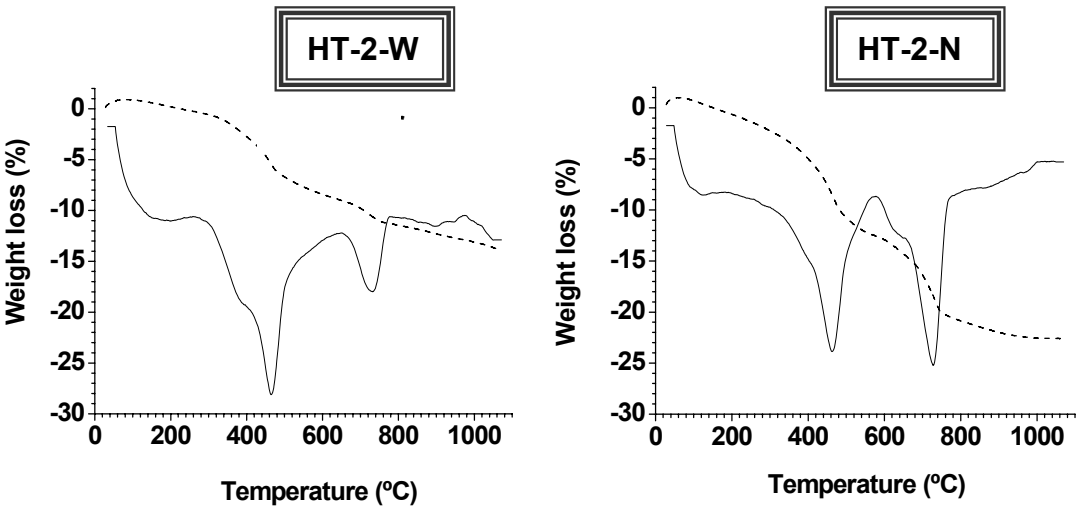

Figure 2. TG and DTG curves of hydrated precursors HT-2-W and HT-2-N

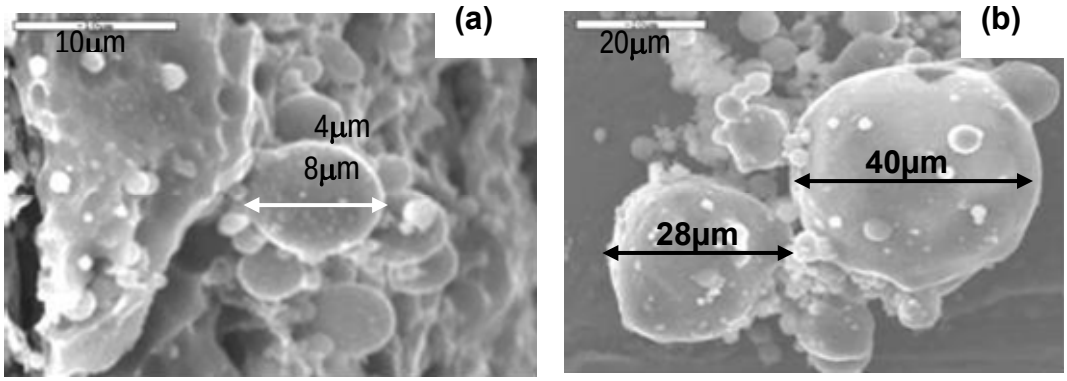

Figure. 3. SEM images of starting fly ash (FA-2).

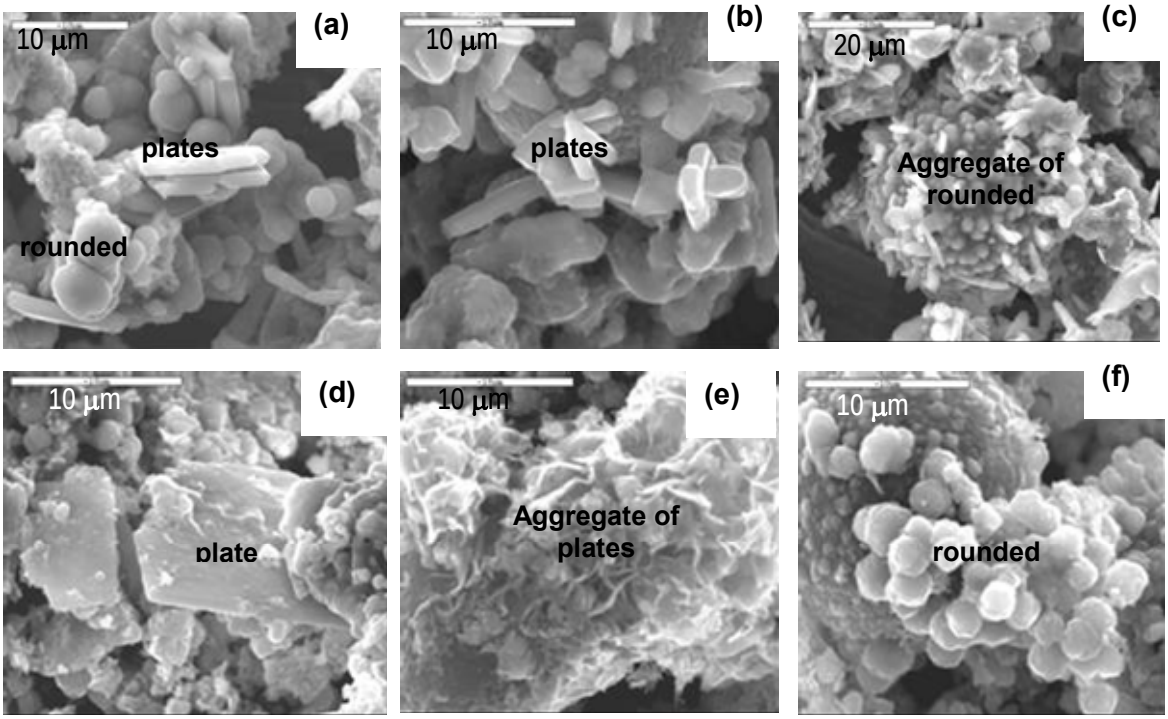

Figure 4. SEM images of anhydrous FABC-2-W (a-c) and FABC-2-N (d-f) cements

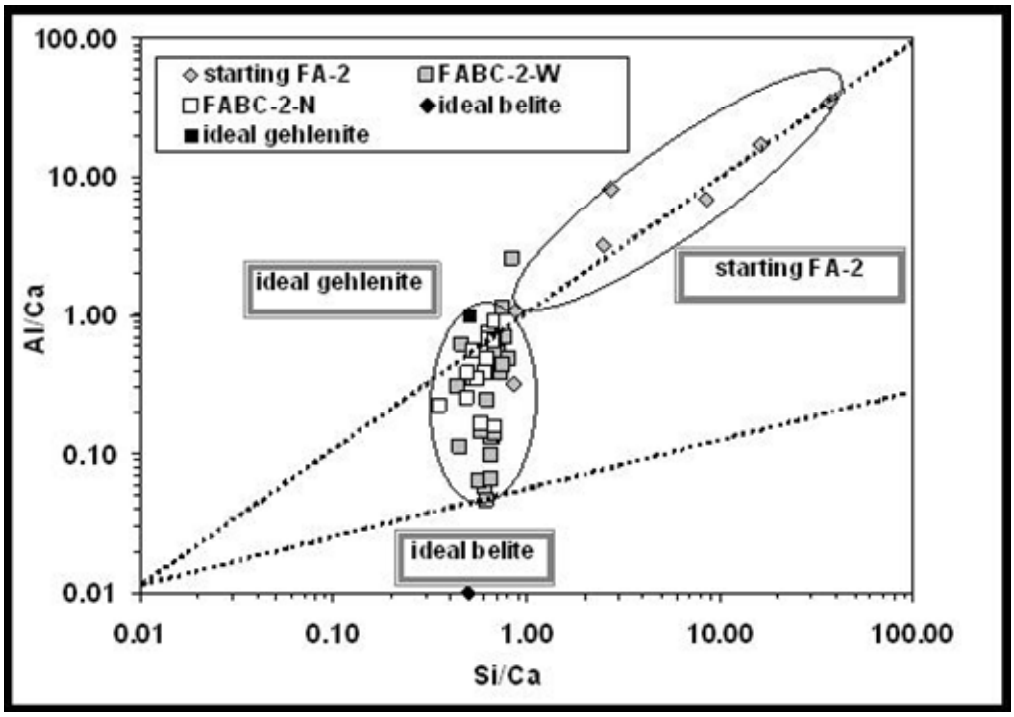

Figura 5. Relaciones atómicas de Al/Ca vs Si/Ca de la ceniza de partida (CV-2), y cementos anhidros (CBCV-2-A y CBCV-2-N).

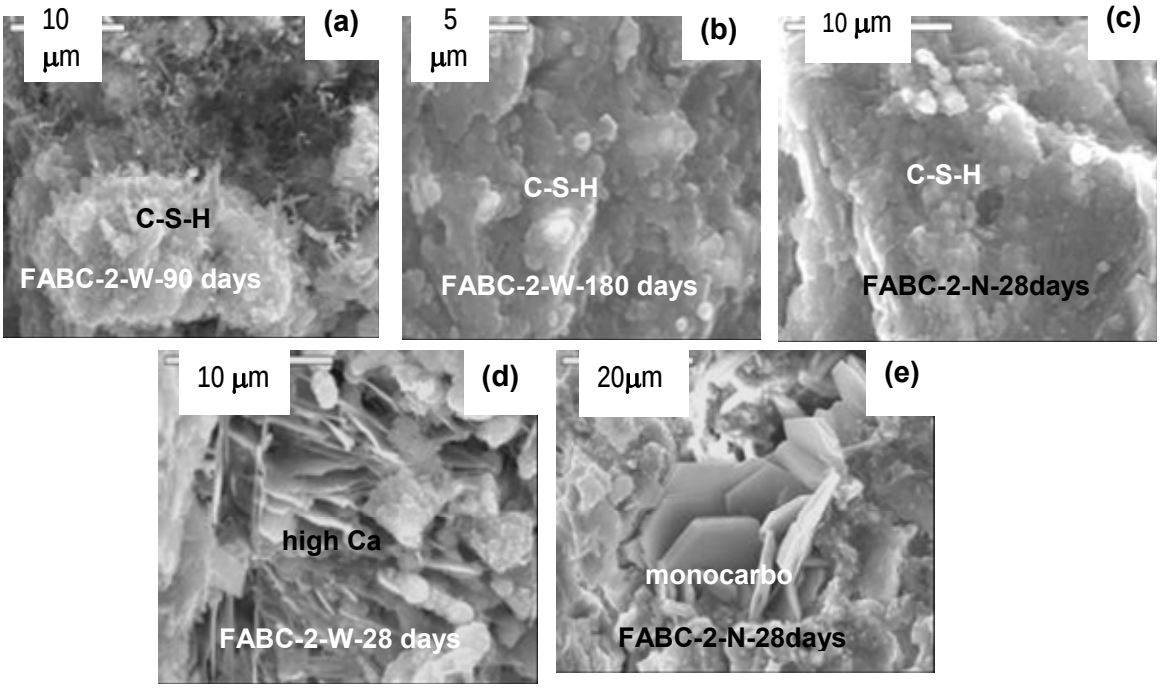

Figure 6. SEM images of hydrated FABC-2-W and FABC-2-N pastes

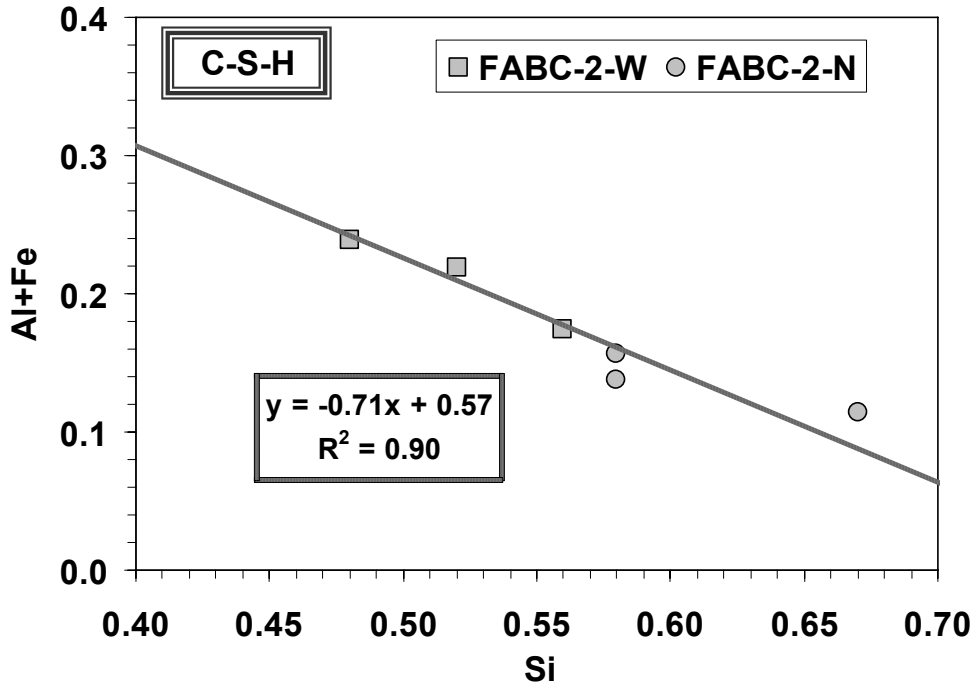

Figure 7. Al+Fe vs Si atom ratio from spot X-ray microanalyses of C-S-H gel of hydrated FABC-2-W and FABC-2-N pastes (Table III).

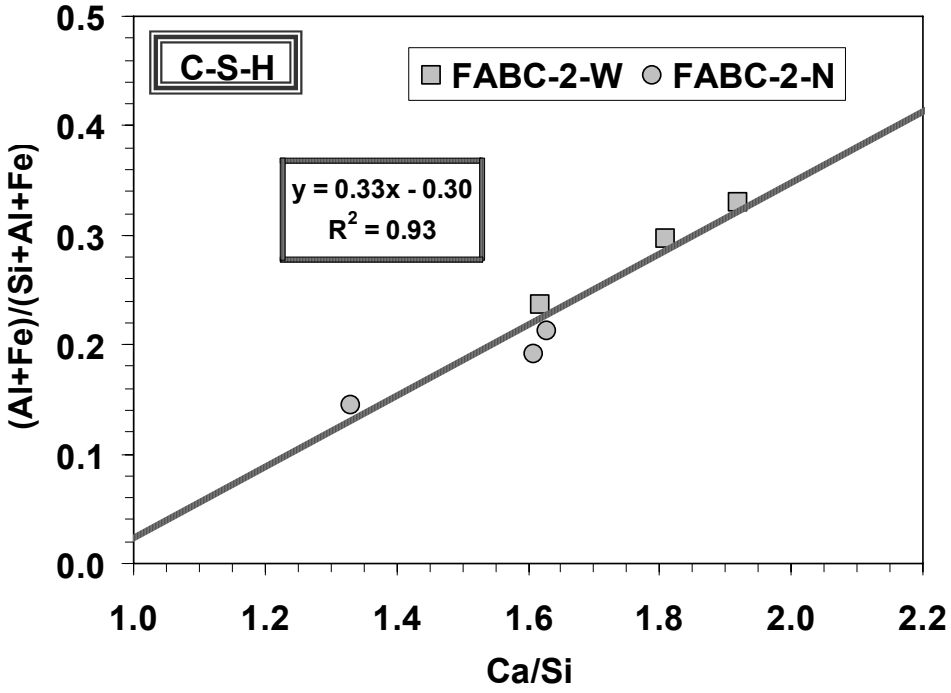

Figure 8. (Al+Fe)/(Si+Al+Fe) vs Ca/Si atom ratio from spot X-ray microanalyses of C-S-H gel of hydrated FABC-2-W and FABC-2-N pastes (Table III).